

# Analytical study on the effects of high dielectric material surrounding spherical sample with coil array for parallel imaging

Wei Luo<sup>1,2</sup>, Giuseppe Carluccio<sup>3</sup>, Zhipeng Cao<sup>1,4</sup>, Yang X Qing<sup>1</sup>, and Christopher M. Collins<sup>1,3</sup>

<sup>1</sup>Radiology, The Pennsylvania State University, Hershey, PA, United States, <sup>2</sup>Engineering Science & Mechanics, The Pennsylvania State University, University Park, PA, United States, <sup>3</sup>Radiology, New York University, New York, NY, United States, <sup>4</sup>Bioengineering, The Pennsylvania State University, University Park, PA, United States

**Introduction:** Previous studies have shown that applying high dielectric material (HDM) in MRI scans can improve local Signal-to-Noise ratio (SNR) and lower transmit power and, therefore, lower the specific absorption rate (SAR), at both 3T and 7T [1-6]. In most of these studies, the size of HDMs and ROI were small compared to the imaging objects, transmit coils, and receive coils. Within this configuration, the effects of HDM can be understood as the magnetic field strength in a region near the HDM is enhanced by the strong displacement current in the HDM, resulting in local improvements in SNR and coil efficiency [1,2]. For coils designed for parallel imaging, often a large number of coils that may be small with respect to the sample is desired [7]. Consequently, coil size may be smaller than the HDM and ROI. In this situation, the effects of HDM have not been well investigated. Here, we use an analytical model to explore the effects of HDM when the coil is smaller than the sample, HDM, and ROI at 3T. Inverse g-factor maps and combined receive sensitivity of an array consisting of eight coils are reported.

**Theory and Method:** A sphere ( $r = 10$  cm) with relative permittivity ( $\epsilon_r = 50$ ) and conductivity ( $\sigma = 0.5$  S/m) of average brain tissue at 3T was used in this study. A dielectric shell (2 cm thick,  $\epsilon_r = 134$ ,  $\sigma = 0$  S/m) encapsulated the sphere. The permittivity and the thickness of dielectric shell were chosen such that the coil efficiency,  $[\|\mathbf{B}_1(\text{ROI})\|/\sqrt{P_{\text{diss}}+P_{\text{coil}}}]$ , was maximized in a 3D ROI shown in Figure 1, where  $\mathbf{B}_1$  denotes the receive sensitivity of a coil,  $P_{\text{diss}}$  and  $P_{\text{coil}}$  are the powers dissipated in the lossy sphere and the coil, respectively. Eight coils were located on surfaces tangent to the shell and sphere a fashion shown in Figure 2. The electromagnetic (EM) fields generated by each coil were calculated individually from an analytical solution and combined later for data processing. The EM fields inside the sphere, dielectric shell, and outside the shell are found using a general solution described by double Fourier series of vector spherical wave functions [8],  $\mathbf{M}_{n,m} = j_n(k\rho) \mathbf{X}_{n,m}(\theta,\varphi)$  and  $\mathbf{N}_{n,m} = (1/k) \nabla \times j_n(k\rho) \mathbf{X}_{n,m}(\theta,\varphi)$ , where  $n, m$  are the expansion indices,  $k$  is the complex wave number,  $j_n$  is the spherical Bessel function of order  $n$ , and  $\mathbf{X}_{n,m}$  is the vector spherical harmonic. In different regions, the EM solutions have different unknown amplitudes which could be solved by appropriate boundary conditions. Based on the receive sensitivity and the coil noise matrix  $\mathbf{R}$ , the combined receive sensitivity map of these eight coils was defined and calculated as [9]  $[(\mathbf{B}_1)^T \mathbf{R}^{-1} (\mathbf{B}_1)^*]^{1/2}$  in the transverse plane with and without dielectric shell, where T denotes the matrix transpose and asterisk denotes the complex conjugate. The coil noise matrix was calculated as  $\mathbf{R}_{ij} = \int \sigma \mathbf{E}_i \cdot \mathbf{E}_j^* dV$ , where  $\mathbf{E}_i$  is the electric field generated by coil  $i$ . To evaluate the parallel performance of these eight coils with the dielectric shell, SENSE g-factor maps in Cartesian  $k$ -space sampling with reduction factors 2, 3, and 4 on the transverse plane were calculated as [10]  $g_p = \{[(\mathbf{B}_1)^H \mathbf{R}^{-1} \mathbf{B}_1]^{-1}_{p,p} [(\mathbf{B}_1)^H \mathbf{R}^{-1} \mathbf{B}_1]_{p,p}\}^{1/2} \geq 1$ , where  $p$  counts a set of pixels that alias in conventional reconstruction and H indicates the transposed complex conjugate.

**Results and Discussion:** The combined receive sensitivity with the dielectric shell out performs than the one without, as shown in Figure 3. The receive sensitivity is enhanced by 38.2% on average and by 43.7% at the center. The parallel performance of the array is slightly better without dielectric shell, reflected from the average value of inverse g-factor and the value at the center shown in Figure 4. The average value of inverse g-factor is degraded by 6.6% at the most and 18.8% at the center. Even with the degraded performance in inverse g-factor, the gains from combined receive sensitivity can still give a promising improvement in SNR when imaging with HDM that is much larger than the coil element size in an array. In imaging of human subjects, where the subject is larger than the ROI and HDM pads, even greater gains in sensitivity may be expected.

**Acknowledgement:** Funding through NIH R01 EB000454.

**References:** [1] Yang *et al.*, JMRI 2006; 24:197–202. [2] Yang *et al.*, MRM 2011; 65:358–362. [3] Haines *et al.*, JMRI 2010;203:323–327. [4] Teeuwisse *et al.*, MRM 2012;67:912–918. [5] Luo *et al.*, MRM 2012, doi 10.1002/mrm.24433. [6] Heer *et al.*, MRM 2012; 68:1317-1324. [7] Wiggins *et al.*, MRM 2009;62:754-762. [8] Keltner *et al.*, MRM 1991;22:467-480. [9] Roemer *et al.*, MRM 1990; 16:192-225. [10] Pruessmann *et al.*, MRM 1999;42:952–962.

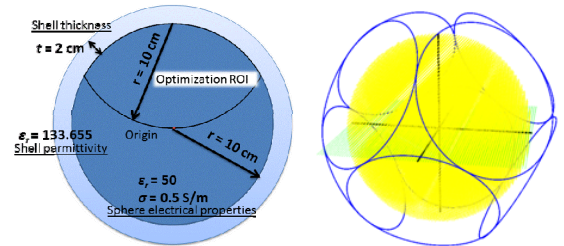


Fig. 1. Spherical model used in this study with its electrical properties and dimensions.

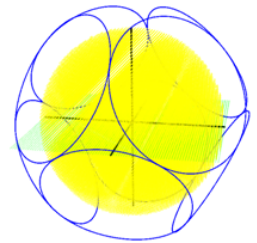


Fig. 2. Coil arrangement of the array used in this study with 8 elements.

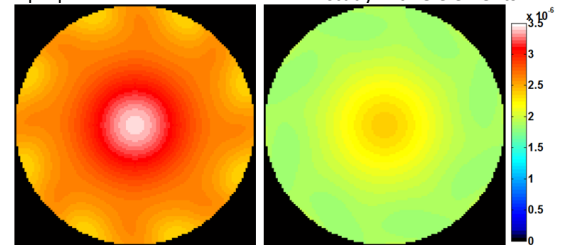


Fig. 3. Combined receive sensitivity with (left) and without (right) the dielectric shell.

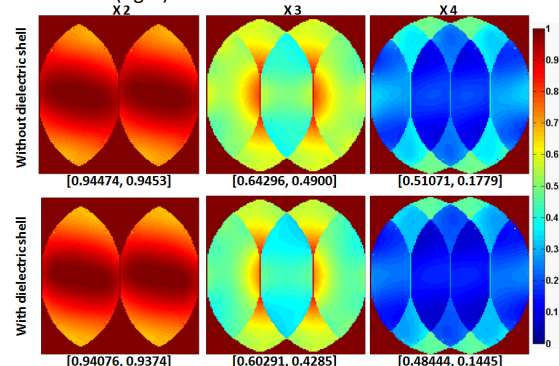


Fig. 4. Inverse g-factor maps with (bottom row) and without (top row) the dielectric shell at different reduction factors, indicated on top of each column. Average value (left) of inverse g-factor and the value at the center (right) are shown in the bracket below each map.